International Journal of Solids and Structures 51 (2014) 3570–3578

Contents lists available at ScienceDirect

International Journal of Solids and Structures

journal homepage: www.elsevier.com/locate/ijsolstr

Compact model and identification process for friction induced damping in a rotational joint with flawed surfaces

N. Bouchaala [a,b,*], N. Peyret [a], I. Tawfiq [a], J.L. Dion [a], M. Haddar [b]

[a] Laboratoire d'Ingénierie des Systèmes Mécaniques et des Matériaux (LISMMA), Supmeca, 3 rue de Fernand Hainaut, 93407 Saint- Ouen Cedex, France
[b] Dynamics of Mechanical Systems Research Unit, National School of Engineers of Sfax, BP 1173-3038 Sfax, Tunisia

ARTICLE INFO

Article history:
Received 30 October 2013
Received in revised form 16 May 2014
Available online 24 June 2014

Keywords:
Damping
Friction
Rotational joint
Analytical compact model
Greenwood model

ABSTRACT

It is well known that bolted joints have significant influence on the dynamical behavior of assembled structures due to formation of damping. This paper focuses on damping caused by dry friction in a rotational joint. Friction can be either induced by micro-slipping or macro-slipping. This paper describes the design of a new experimental device intended to measure damping caused by friction and partial slip in rotational joints. An original method for measuring dissipated energy in rotational joints with plan-plan contact is proposed. This method is based on Lagrange formalism and allows to measure accurately forces and torques only with accelerometers. These techniques are available for very small displacements that occur in micro-slip and partial slip of surfaces in contact and are still available for large displacements (macro-slip). An analytical compact model based on the Greenwood model is studied. The experimental results and simulations used to quantify the dissipated energy in order to compute the damping ratio are presented and discussed.

1. Introduction

For design reasons, and also due to handling and maintenance, all jointed structures must be assembled in the same way, by welding, bolting and riveting. The presence of the joint is a major source of energy dissipation that is often badly predicted (Davies et al., 2012). Mechanical connections (bolted or riveted) are widely used in aerospace, railway, automotive structures and also in many mechanical components (bridges, cranes) to ensure the load transfer from one structural element to another.

The behavior of a bolted connection is non-linear and often relative movements, or micro sliding called fretting, occurs between two pieces and therefore to energy dissipation (Eriten et al., 2010, 2011) and (Dini and Hills, 2009) through Coulomb friction.

Over the years, much research has been dedicated to friction problems in jointed structures and mention can be made of the work of Peyret et al., 2010. In assembled structures, damping is caused by macro-slipping (Berthillier et al., 1998; Poudou, 2007) or by micro-slipping (Goodman and Klumpp, 1956; Beards and Williams, 1977; Rao et al., 2010). Blau (1992) defined micro-slips as "Small relative tangential displacements in a contacting area at an interface, when the remainder of the interface in the contacting area is not relatively displaced tangentially". In contrast, macro-slip takes place when the whole contacting area undergoes a relative displacement.

There are two distinct sources of damping in assembled structures. The first is damping in the materials of the assembly; the second is damping in the joints (Bhagat and Bijoy, 2012; Nanda, 2006), which is difficult to evaluate. Compared to material damping, bolted or riveted joints are the primary source of damping if no special damping treatment is added to the structure. The damping value of the material is already known and often lower than the damping value in assembled structures (Poudou, 2007; Ibrahim and Pettit, 2005; Caignot et al., 2005; Beards and Williams, 1977).

In their studies of bolted joints, several authors have used experimental setups to highlight friction induced damping: Dion et al. (2012) proposed a clamped–clamped beam excited on its first bending mode. The beam was built with three parts linked by two planar joints. Ahmadian and Jalali (2007) worked on a structure composed of two beams assembled by a single bolted joint. Their structure was studied under free conditions on its first bending mode. Ouyang et al. (2006) presented experimental results for a single bolted joint excited by a torsional dynamic load. Beards and Williams (1977) worked on structures with rotational slips in joints. This type of device avoided coupling between normal and tangential stress and provided better control of the normal load.

* Corresponding author at: Dynamics of Mechanical Systems Research Unit, National School of Engineers of Sfax, BP 1173-3038 Sfax, Tunisia. Tel.: +216 93509503.
E-mail address: noussabouchaala@gmail.com (N. Bouchaala).

http://dx.doi.org/10.1016/j.ijsolstr.2014.06.014
0020-7683/

The aim of this work is to study the phenomenon of energy dissipated by sliding between two nominally flat surfaces subjected to normal force and alternated rotation. The experimental device is designed for a wide range of sliding amplitudes. This benchmark was designed to simulate the behavior of a bolted joint under rotational slip, like for example the poly-articulated structure with rotating friction joints from Beards and Williams (1977) and the beam assembly with an active rotative joint from Gaul (2000). Section 2 describes the experimental device designed and studied to reveal this phenomenon. In the experimental work the excitation force is applied orthogonally to the bolt axis using a small electrodynamic shaker. The response of the assembled structure is measured by three accelerometers. The experimental method is developed in Section 3. Lagrange formalism is used for the hysteresis loops of torque-angular displacement (rotation) to obtain the equation of motion of the system. A new method of post-processing experimental signals (based on kinetic equations) in order to transform the tangential accelerations (given by accelerometer) in angular acceleration is presented. Experimental torque-angular displacement (rotation) plots at the joint highlight hysteresis loops which can be used to estimate the damping dissipation at the joint. In Section 4 the Greenwood model is extended to friction surfaces in rotation. The main interest of this extension consists in the technology of rotational joints and bolted joints that often produce such kind of friction. A compact contact model and numerical results are presented. The experimental results and simulations are compared in Section 5.

2. Experimental device

To study the phenomenon of energy dissipated by Coulomb friction due to micro slip in bolted joint, we used the experimental device shown schematically in Fig. 1. The experimental setup consists of two vertical beams with an interface provided by a contact surface at the two beams and a bolt. The nominal contact surface is defined by a rectangle (28×18 mm). For this surface, roughness (R_a) is lower than 0.2 μm (see Fig. 2). The geometrical characteristics of the beams are given in Fig. 3. The free-free structure is excited by a shaker attached to the structure via a rod screwed into both the shaker and the upper beam. The power supply generating the response of the mini-shaker is provided by a signal generator passing through an amplifier. The excitation force is applied to point D and the response of the assembled structure is measured at points A, B and C through three accelerometers (Fig. 1). Therefore the excitation force applied at point D in Fig. 1 will produce a torque in the same plane of the joint interface. The bolt is tightened with a fixed preload that assumed constant during the experimental measurements; this latter is controlled during the experiment by an annular force sensor. The signals from the accelerometers are post processed by the analyzer software.

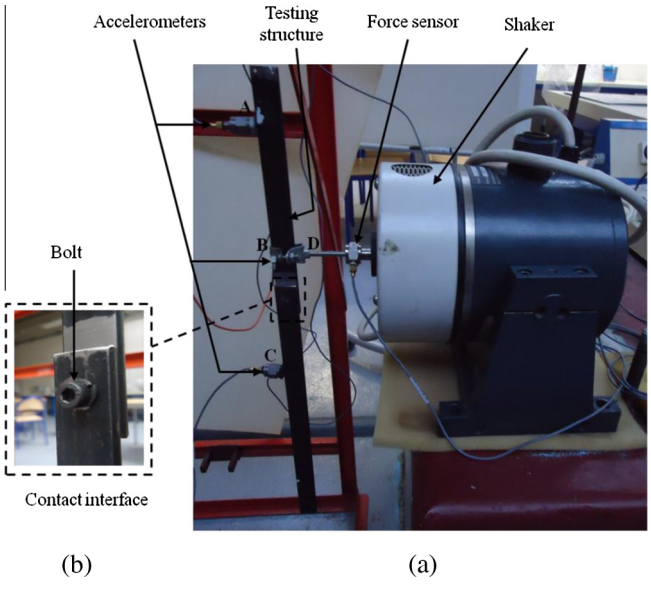

Fig. 1. Experimental device: (a) test set up with a shaker and testing structure, (b) lap joint.

In order to choose the excitation frequency, the eigenfrequencies of the system (Table 1) are obtained using a finite element model built with **ANSYS**. The excitation frequencies tested are all between 5 and 50 Hz.

The instrumentation of the experimental set up is used to measure the accelerations and the excitation force (Fig. 4). The force exerted by the shaker is measured by a force sensor placed at point D (Fig. 1) with a sensitivity of 100 mv. The vibrations thus generated are detected by three accelerometers placed at points A, B and C, whose sensitivities are 10.35 mv/g, 10.79 mv/g and 10.29 mv/g, respectively (where g is the gravitational acceleration).

3. Experimental results

3.1. Experimental method

The objective of the experimental study is to quantify the energy dissipated by dry friction due to micro-sliding introduced in the link in order to compute the damping ratio. To achieve this aim, two steps are necessary to measure accurately forces and torques only with accelerometers.

- The first is to determine the equation of motion of the system to express the torque according to the angles of rotation (degrees of freedom of the structure).
- The second step involves post processed signals delivered by accelerometers in order to transform the tangential accelerations (given by accelerometer) in angular acceleration) and then integrated in the equations of motion of the system to determine the hysteresis loops, i.e. the torque according to the angles of rotation.

Finally, the energy dissipated by friction at the links is given by the inner surface of the hysteresis loops.

To better explain the problem, the methodology is given in Fig. 5.

3.2. Equation of motion of the structure

We used Lagrange formalism to obtain the equations of motion of the structure. The structure is shown in Fig. 6. Three independent parameters θ_1, θ_2 and x_1 are needed to describe the motion of the structure.

- Kinetic energy

In the first step, we define the kinetic energy of the system:

$$Ec = \frac{1}{2}m_1 V_{G1}^2 + \frac{1}{2}I_1\dot{\theta}_1^2 + \frac{1}{2}m_2 V_{G2}^2 + \frac{1}{2}I_2\dot{\theta}_2^2 \quad (1)$$

with

m_i: the mass of the beam i $(i = 1, 2)$
I_i: moment of inertia of the beam i $(i = 1, 2)$
θ_i: angular displacement of the beam i $(i = 1, 2)$
V_{G1}: the velocity of the center of mass of beam1 given by:

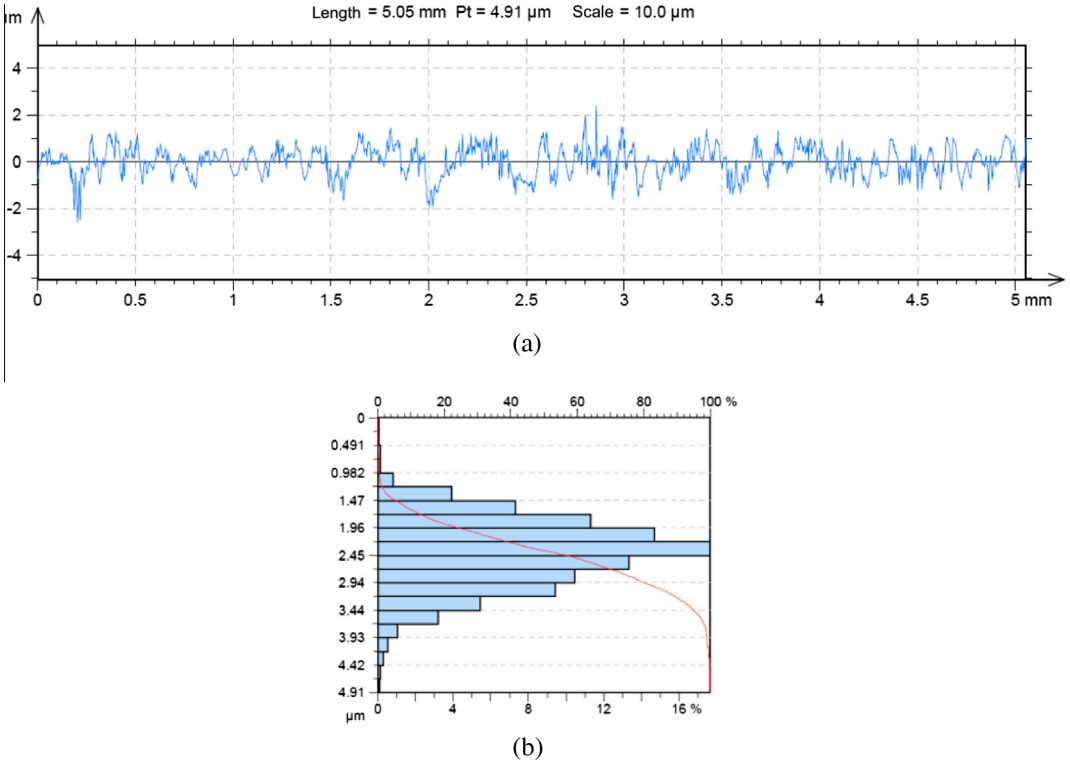

Fig. 2. Roughness of surface (a) description of roughness, (b) probability density of roughness.

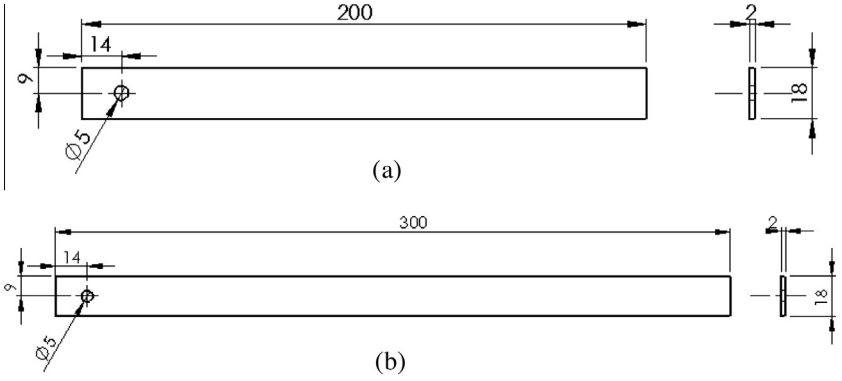

Fig. 3. Geometric characteristics of the beams (a) top beam, (b) lower beam.

Table 1
Eigenfrequencies of the system.

Mode	1	2	3	4	5	6
Frequency (Hz)	99.72	270.83	476.81	529.02	913.91	1156

$$\overrightarrow{V_{G1}} = \dot{x}_1 \overrightarrow{X_0} \tag{2}$$

with

x_1: the displacement of the center of gravity of the beam due to the higher driving force of the shaker.

V_{G2}: the velocity of the center of mass of beam 2 given by:

$$\overrightarrow{V_{G2}} = \left(\dot{x}_1 + \left(\frac{l_1}{2} - h\right)\dot{\theta}_1 \cos\theta_1 + \left(\frac{l_2}{2} - h\right)\dot{\theta}_2 \cos\theta_2\right)\vec{X}_0 - \left(\left(\frac{l_1}{2} - h\right)\dot{\theta}_1 \sin\theta_1 + \left(\frac{l_2}{2} - h\right)\dot{\theta}_2 \sin\theta_2\right)\vec{Z}_0 \tag{3}$$

Hence the kinetic energy given by:

$$E_c = \frac{1}{2}m_1\dot{x}_1^2 + \frac{1}{2}I_1\dot{\theta}_1^2 + \frac{1}{2}m_2\dot{x}_1^2 + m_2\dot{x}_1\dot{\theta}_1\left(\frac{l_1}{2} - h\right)\cos\theta_1 + \frac{1}{2}m_2\left(\frac{l_1}{2} - h\right)^2\dot{\theta}_1^2 + \frac{1}{2}m_2\left(\frac{l_2}{2} - h\right)^2\dot{\theta}_2^2 + m_2\dot{x}_1\dot{\theta}_2\left(\frac{l_2}{2} - h\right)\cos\theta_2 + m_2\left(\frac{l_2}{2} - h\right)\left(\frac{l_1}{2} - h\right)\dot{\theta}_1\dot{\theta}_2 \times \cos(\theta_1 - \theta_2) + \frac{1}{2}I_2\dot{\theta}_2^2 \tag{4}$$

- Potential energy

In the second step, we define the potential energy of the system:

$$E_p = m_2 g\left(\frac{l_2}{2} - h\right)(1 - \cos\theta_2) + m_2 g\left(\frac{l_1}{2} - h\right)(1 - \cos\theta_1) \tag{5}$$

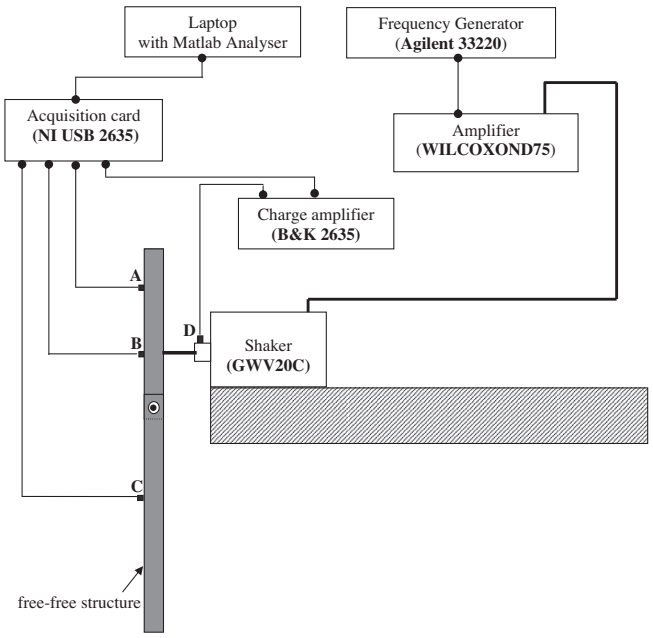

Fig. 4. Diagram of the data acquisition device.

- Lagrangian formalism

Three independent parameters θ_1, θ_2, x_1 are needed to describe the motion of the system. In this case the Lagrange equations applied to the system (see Appendix A) can be written as:

$$\begin{cases} M_F = (I_1 + m_2 d_3^2)\ddot{\theta}_1 + m_2 d_3 \ddot{x}_1 \cos\theta_1 + m_2 d_3 d_5 \ddot{\theta}_2 \cos(\theta_1 - \theta_2) + m_2 d_3 d_5 \dot{\theta}_2^2 \sin(\theta_1 - \theta_2) + m_2 g d_3 \sin\theta_1 \\ M = (I_2 + m_2 d_5^2)\ddot{\theta}_2 + m_2 d_5 \ddot{x}_1 \cos\theta_2 + m_2 d_3 d_5 \ddot{\theta}_1 \cos(\theta_1 - \theta_2) - m_2 d_3 d_5 \dot{\theta}_1^2 \sin(\theta_1 - \theta_2) + m_2 g d_5 \sin\theta_2 \\ F = (m_1 + m_2)\ddot{x}_1 + m_2 d_5 \ddot{\theta}_2 \cos\theta_2 - m_2 d_5 \dot{\theta}_2^2 \sin\theta_2 + m_2 d_3 \ddot{\theta}_1 \cos\theta_1 - m_2 d_3 \dot{\theta}_1^2 \sin\theta_1 \end{cases} \quad (6)$$

With

F: the driving force of the shaker
M: the torque
M_F: the torque of force F

$$d_3 = \left(\frac{l_1}{2} - h\right) \text{ and } d_5 = \left(\frac{l_2}{2} - h\right) \quad (7)$$

In the rest of this paper we are interested in using the expression of torque as a function of rotation angles.

$$M = (I_2 + m_2 d_5^2)\ddot{\theta}_2 + m_2 d_5 \ddot{x}_1 \cos\theta_2 + m_2 d_3 d_5 \ddot{\theta}_1 \cos(\theta_1 - \theta_2) - m_2 d_3 d_5 \dot{\theta}_1^2 \sin(\theta_1 - \theta_2) + m_2 g d_5 \sin\theta_2 \quad (8)$$

I_1 and I_2 are the moments of inertia of the beam given by the Huygens theorem.

$$I_1 = m_1 \frac{l_1^2}{12} + m_c d_1^2 \quad (9)$$

$$I_2 = m_2 \frac{l_2^2}{12} + m_c d_4^2 \quad (10)$$

m_c: mass of the sensor (m_c = 9.94 g).

3.3. Post treatment

In this work, a new method of post-processing of experimental signals based on kinetic equations is developed. To integrate the signals delivered by the accelerometers in the motion equation of the system (Eq. (8)), we have to transform the tangential accelerations in angular acceleration. Consequently we chose to use the kinematic equations (see Appendix B).

3.4. Experimental results

In order to plot the experimental hysteresis loops in the torque-angular rotation from the signals delivered by the accelerometers we use the following algorithm (Fig. 7):

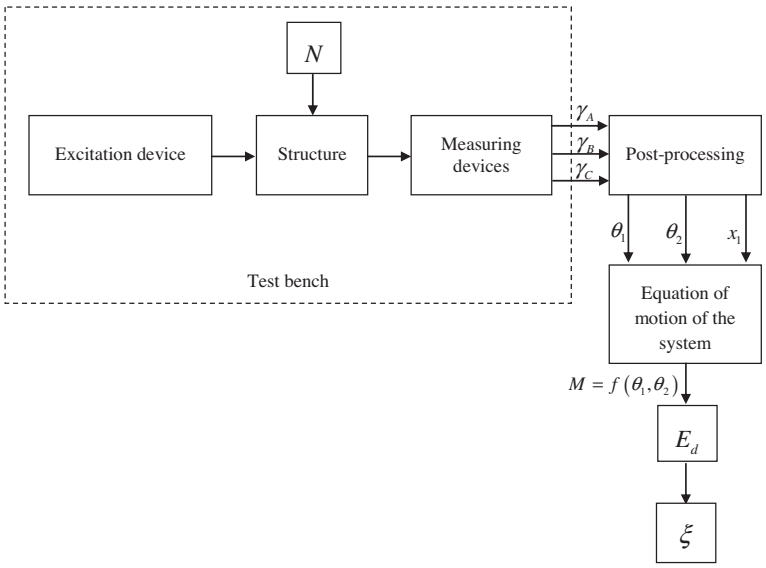

Fig. 5. Diagram of the experimental study.

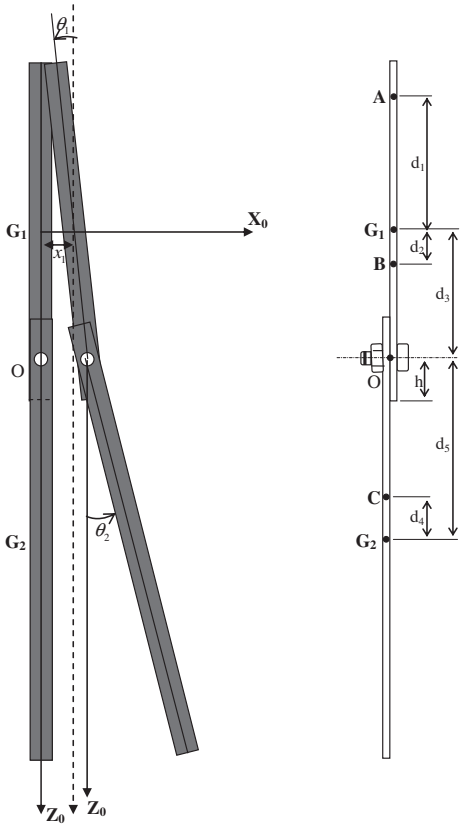

Fig. 6. The parameters of the structure.

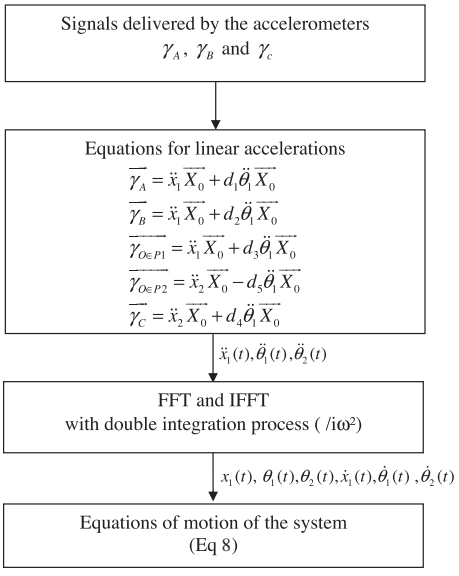

Fig. 7. Algorithm considered for the representation of hysteresis loops obtained from the experimental measurements.

For the torque-angular displacement hysteresis loops, a first integration and second integration of the acceleration signals are necessary to obtain the velocity and displacement. A Fourier transforms (FFT) and an inverse Fourier transform (IFFT) are used in the algorithm (Fig. 7) to integrate the acceleration signals (response of the accelerometers). The hysteresis loops obtained from the experimental results of torque versus angular displacements at 100 N (preload) subjected to different levels of amplitude of excitation (excitation amplitude delivered by the shaker) are presented in

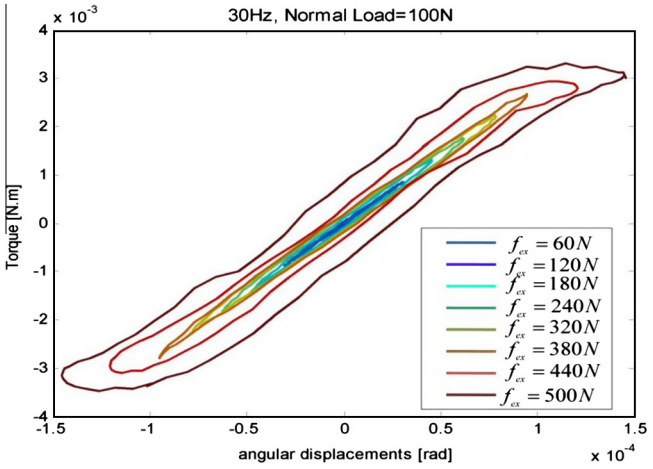

Fig. 8. Experimental hysteresis loops: torque as a function of the angular displacements.

Fig. 8. The range variation of the excitation force is between 60 N and 500 N. The excitation frequency is 30 Hz and the normal stress due to the tightening torque of the bolt is 100 N. Depending on the preload on the bolt, non-linear dynamical effects due to dry friction can be expected at the area of contact of the beams caused by the hysteresis loops in the torque-angular rotation the first time, and due to micro-slip caused by the looseness of the joint the second time. The area inside the curve is the dissipated energy during micro-slip per cycle. The oblique part of the curve represents the tangential stiffness.

4. Theoretical models

The modeling of the contact between two rough surfaces (Fig. 9a) is based on the hypothesis proposed by Robbe-Valloire et al. (2000), which reduces the problem to a contact between a rough surface (equivalent at the roughness of the two surfaces in contact) and a rigid plane (Fig. 9b).

Consider the elastic contact between a rigid plane and a rough surface composed of a multitude of asperity. The compact contact model **EGM** (Extended Greenwood model) with micro-contacts and statistical distributions was developed and studied in previous works; see Bouchaala et al. (2013). Using this model as the basis, in this paper we consider the contact between a rigid plane and a nominally flat surface first subjected to a constant normal force N, then to an oscillating angular displacement θ_t. It will be assumed that the coefficient of sliding friction μ between the surfaces is a constant and that dry friction is modeled by Coulomb's law. We assume that all asperity summits are spherical with the same radius ρ and that their heights vary randomly $\varphi(y_i)$. Fig. 10 gives a schematic presentation of the type of contact considered.

Assuming that the probability density function $\varphi(y_i)$ for asperity heights following Gaussian distribution is given by:

$$\varphi(y_i) = \frac{1}{\sigma\sqrt{2\pi}} e^{-\frac{(y_i-m)^2}{2\sigma^2}} \tag{11}$$

where m (location of the peak) is the mean and σ^2 is the variance

Firstly, we consider the model of a contact between an individual spherical asperity and a rigid plane. The contact model adopted is shown in Fig. 11. It is assumed that the elastic proprieties of the contacting bodies are identical to an equivalent elastic material on a rigid plane (Mindlin, 1949). The frictional load is parallel to axis x.

The behavior of an individual asperity can be derived from the Hertzian equations. For the contact between a sphere of radius ρ

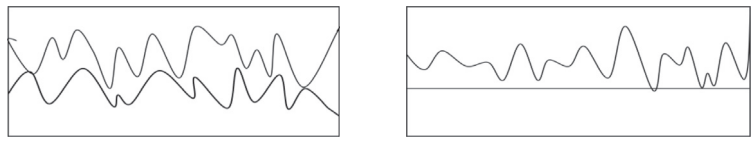

(a) Contact between two rough surfaces

(b) Contact between a rough surface and a rigid plane

Fig. 9. Contact between two surfaces.

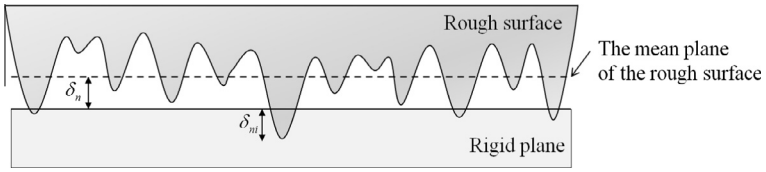

Fig. 10. Contact between a rough surface and a rigid plane.

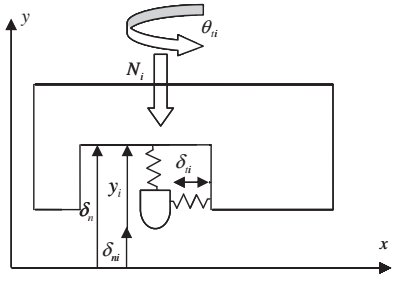

Fig. 11. The contact model for a single asperity.

and a rigid plane, the contact radius a_i and load N_i can be expressed in terms of the compliance δ_{ni} by Greenwood and Williamson (1966):

$$N_i = \frac{4}{3}\sqrt{\rho}E^*\delta_{ni}^{3/2} \tag{12}$$

$$a_i = \sqrt{\rho\delta_{ni}} \tag{13}$$

where E^* is a composite modulus of elasticity given by:

$$\frac{1}{E^*} = \frac{1-\upsilon_1^2}{E_1} + \frac{1-\upsilon_2^2}{E_2} \tag{14}$$

The angular displacement θ_{ti} is given by:

$$\theta_{ti} = \frac{\delta_{ti}}{r_i} \tag{15}$$

where δ_{ti} is the tangential displacement and r_i the radius of the place of the asperity (Fig. 11).

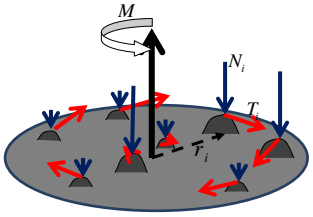

Fig. 12. Sketch of contact areas, loading and sliding.

Fig. 12 shows the sketch of the loading and sliding contact areas. The closer the contact areas are to the center (due to geometric faults) the more probable it is that they will be subject to micro sliding. For the furthest contact areas, macro sliding becomes more predictable; however, the higher the load on the contact areas, the more probable it is that they will be subject only to micro sliding.

The torque moment M_i supported by asperities is given by:

$$M_i = r_i T_i \tag{16}$$

where T_i is the tangential load supported by the asperities.

For an oscillating tangential displacement δ_{ti} with constant amplitude, the tangential load is given by the following equations (Bouchaala et al., 2013):

– During loading $(\dot{\delta}_{ti} > 0)$

$$T_i = \mu N_i\left(1 - \left(1 - \frac{16a_i\delta_{ti}}{3\mu N_i G^*}\right)^{3/2}\right) \tag{17}$$

– During unloading $(\dot{\delta}_{ti} < 0)$

$$T_{id} = 2\mu N_i\left(\left(0.5\left(\frac{16a_i\delta_{ti}}{3\mu N_i G^*} + \left(1 - \frac{T_{i\max}}{\mu N_i}\right)^{3/2} + 1\right)^{3/2}\right) - 1\right) + T_{i\max} \tag{18}$$

– During reloading $(\dot{\delta}_{ti} > 0)$

$$T_{ic} = -T_{id}(-\delta) = -2\mu N_i\left(\left(-0.5\left(\frac{16a_i\delta_{ti}}{3\mu N_i G^*} - \left(1 - \frac{T_{i\max}}{\mu N_i}\right)^{3/2} - 1\right)^{3/2}\right) - 1\right) - T_{i\max} \tag{19}$$

where G^* is expressed by:

$$G^* = \left(\frac{2-\nu_1}{G_1} + \frac{2-\nu_2}{G_2}\right) \tag{20}$$

G is the shear modulus. Indices 1 and 2 refer to the two bodies in contact.

According to Eq. (16), and taking into account Eqs. (17)–(19), the expression of rotation moment M_i is defined by:

– During loading $(\dot{\theta}_{ti} > 0)$

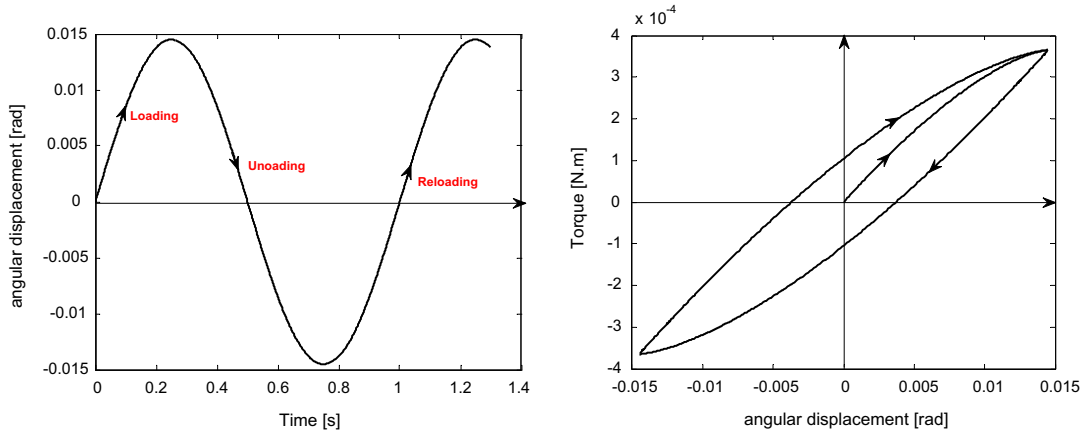

Fig. 13. (a) The loading path. (b) Hysteresis loops: torque as a function of the angular displacements for a single asperity.

$$M_i = r_i \mu N_i \left(1 - \left(1 - \frac{16 a_i r_i \theta_{ti}}{3 \mu N_i G^*}\right)^{3/2}\right) \tag{21}$$

– During unloading ($\dot{\theta}_{ti} < 0$)

$$M_{id} = 2 r_i \mu N_i \left(\left(0.5\left(\frac{16 a_i r_i \theta_{ti}}{3 \mu N_i G^*} + \left(1 - \frac{(r_i T_i)_{\max}}{\mu N_i}\right)^{3/2} + 1\right)^{3/2}\right) - 1\right) + (r_i T_i)_{\max} \tag{22}$$

– During reloading ($\dot{\theta}_{ti} > 0$)

$$M_{ic} = -2 r_i \mu N_i \left(\left(-0.5\left(\frac{16 a_i r_i(\theta_{ti})}{3 \mu N_i G^*} + \left(1 - \frac{(r_i T_i)_{\max}}{\mu N_i}\right)^{3/2} - 1\right)^{3/2}\right) - 1\right) - (r_i T_i)_{\max} \tag{23}$$

For an oscillating angular displacement θ_{ti} (Fig. 13(a)) and during loading, unloading and reloading, the hysteresis loops of the "torque/angular displacement" relation for a single asperity are shown in Fig. 13(b).

Secondly, we consider the contact between a rigid flat surface and a rough surface using GW models (Bouchaala et al., 2013) (Fig. 9). The reference plane defined by the mean height of the asperities and the rigid flat surface are separated by a distance, δ_n.

To study this type of contact, we adopted the following assumptions:

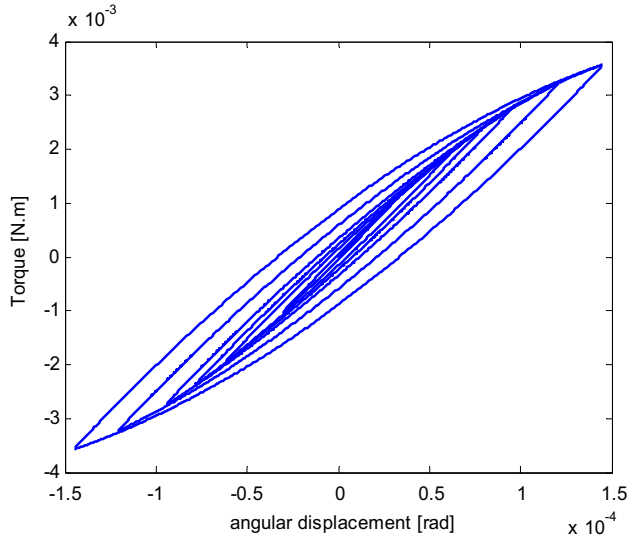

Fig. 14. Hysteresis loops: torque as a function of angular displacements.

– A Gaussian distribution of asperity heights;
– The total normal load N applied to the contact between a plane and a nominally flat surface (Fig. 10) can be expressed as the sum of each elementary normal load on each asperity N_i;

$$N = \sum N_i \tag{24}$$

– A equiprobable distribution of asperity in angular rotation θ and a affine distribution for the radial distance r_i to the center of rotation.
– Keeping N constant, the loading cycle, which is angular displacement θ_t, oscillates between $\theta_{t\max}$ and $(-\theta_{t\max})$ applied to the contact. The total torque that can be borne by N_a asperities is:

$$M = \sum M_i = \sum r_i T_i \tag{25}$$

By keeping N constant and increasing the amplitude of the angular displacement per iteration, the hysteresis loops of the torque-angular displacement relations for a contact are shown in Fig. 14.

5. Results and validation

In accordance with the experimental results, the numerical simulations are performed with the parameters given in Table 2. In Fig. 15, the theoretical model is simulated with friction coefficient μ and roughness R_a of the structure studied compared with the experimental results. It can be seen clearly that the shapes of the hysteresis loop obtained by the theoretical model are quite different from that obtained experimentally. However the scope of this work is to predict damping caused by friction with the aim of producing a model capable of describing the energy loss and damping ratio.

5.1. Dissipated energy

The purpose of this section is to define dissipated energy E_d in order to compute the damping ratio. The area enclosed by the

Table 2
Numerical simulations parameters.

m	$m = 2.45$ μm
σ	$\sigma = 0.45$ μm
μ: the coefficient of sliding friction	$\mu = 0.15$
E: composite modulus of elasticity	$E_1 = E_2 = 210$ GPa

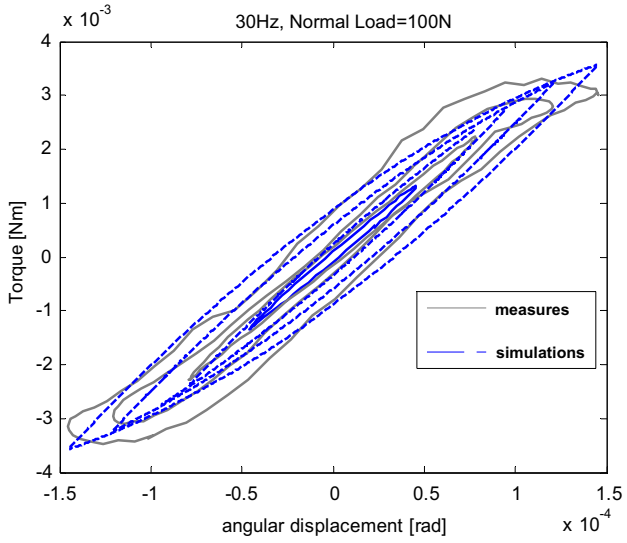

Fig. 15. Theoretical model and measured result.

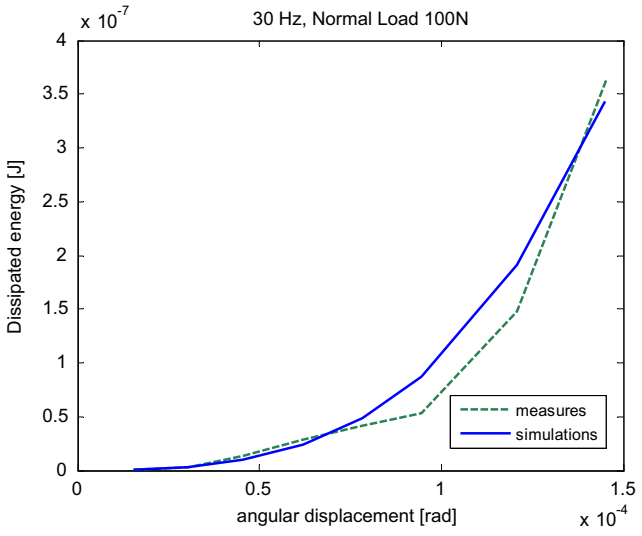

Fig. 16. Evolution of dissipated energy versus the magnitude of angular rotation.

hysteresis loop for periodic signals represents the energy dissipated by dry friction.

Fig. 16 represents the evolution of the dissipated energy versus the magnitude of the angular rotation $(\theta_1 - \theta_2)$ under a normal load 100 N. These curves highlight the nonlinear effect of the interface on dissipated energy: the dissipated energy depends strongly on the angular amplitude of rotation.

5.2. Damping ratio

The damping ratio ξ can be defined by the ratio between the dissipated energy E_d and the supplied energy E_s (Bouchaala et al., 2013):

$$\xi = \frac{4}{\pi}\frac{E_d}{E_s} \tag{26}$$

where the supplied energy E_s for periodic signals is given by the following equation:

$$E_s = 4(\theta_1 - \theta_2)_{\max} M_{\max} \tag{27}$$

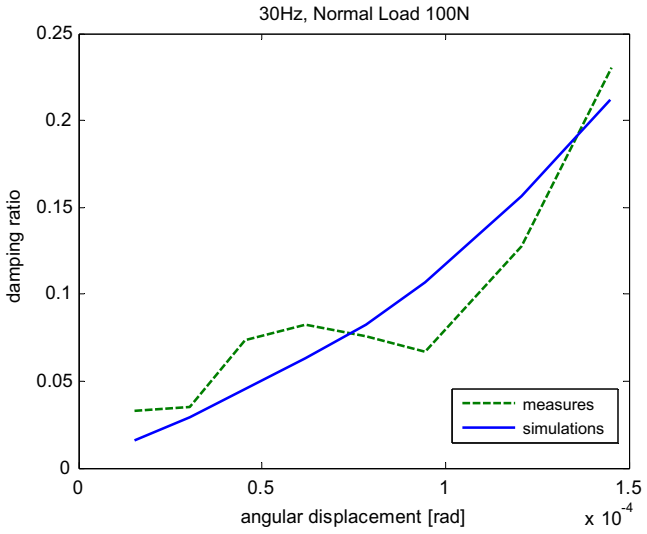

Fig. 17. Evolution of the damping ratio versus magnitude of angular rotation.

The evolution of damping ratio ξ as a function of angular displacement $(\theta_1 - \theta_2)$ is presented in Fig. 17. It can be seen clearly that the damping ratio increases as the angular displacement increases. Therefore it can be concluded that the damping ratio depends on the amplitude of the angular displacement. This dependence induces nonlinear effects which are shown clearly in Fig. 17, since the evolution of the curve is parabolic.

It can be seen clearly that the shapes of the hysteresis loop obtained by the theoretical model are quite different from that obtained experimentally, but the damping model and the simulation of dissipated energy are close to the experimental measurements.

6. Conclusion

This paper presented theoretical and experimental work on an assembled structure with a rotational joint. The experimental device proposed by the authors was designed to quantify the energy dissipated in order to compute the damping ratio at the interface with known and controlled loads for sliding in rotation. This device provides non-linear damping due to micro-slips between the surfaces in contact. A new method of post-processing experimental signals based on Lagrangian formalism and kinematic equations is developed in order to build a compact model for friction induced damping. The hysteresis loops of the torque versus the angular displacement subjected to multiple excitation amplitudes were presented. The compact damping model proposed allows describing friction induced damping due to geometric faults in the surfaces of the contact and avoids the need to provide a full description of their exact geometry. The experimental and numerical results were in agreement and highlighted the nonlinear effect of the interface on dissipated energy and damping.

Appendix A

The Lagrange equations applied to the system can be written as:

$$\begin{cases} \frac{d}{dt}\frac{\partial E_c}{\partial \dot{\theta}_1} - \frac{\partial E_c}{\partial \theta_1} + \frac{\partial E_p}{\partial \theta_1} = M_F \\ \frac{d}{dt}\frac{\partial E_c}{\partial \dot{\theta}_2} - \frac{\partial E_c}{\partial \theta_2} + \frac{\partial E_p}{\partial \theta_2} = M \\ \frac{d}{dt}\frac{\partial E_c}{\partial \dot{x}_1} - \frac{\partial E_c}{\partial x_1} + \frac{\partial E_p}{\partial x_1} = F \end{cases} \tag{A.1}$$

We then obtain the following three equations of motion:

$$\begin{cases} M_F = I_1\ddot{\theta}_1 + m_2\left(\frac{l_1}{2}-h\right)\ddot{x}_1\cos\theta_1 + m_2\left(\frac{l_1}{2}-h\right)^2\ddot{\theta}_1 + m_2\left(\frac{l_2}{2}-h\right)\left(\frac{l_1}{2}-h\right)\ddot{\theta}_2\cos(\theta_1-\theta_2) + m_2\left(\frac{l_2}{2}-h\right)\left(\frac{l_1}{2}-h\right)\dot{\theta}_2^2\sin(\theta_1-\theta_2) + m_2 g\left(\frac{l_1}{2}-h\right)\sin\theta_1 \\ M = I_2\ddot{\theta}_2 + m_2(\frac{l_2}{2}-h)\ddot{x}_1\cos\theta_2 + m_2\left(\frac{l_2}{2}-h\right)^2\ddot{\theta}_2 + m_2\left(\frac{l_2}{2}-h\right)\left(\frac{l_1}{2}-h\right)\ddot{\theta}_1\cos(\theta_1-\theta_2) - m_2\left(\frac{l_2}{2}-h\right)\left(\frac{l_1}{2}-h\right)\dot{\theta}_1^2\sin(\theta_1-\theta_2) + m_2 g\left(\frac{l_2}{2}-h\right)\sin\theta_2 \\ F = (m_1+m_2)\ddot{x}_1 + m_2\left(\frac{l_2}{2}-h\right)\ddot{\theta}_2\cos\theta_2 - m_2\left(\frac{l_2}{2}-h\right)\dot{\theta}_2^2\sin\theta_2 + m_2\left(\frac{l_1}{2}-h\right)\ddot{\theta}_1\cos\theta_1 - m_2\left(\frac{l_1}{2}-h\right)\dot{\theta}_1^2\sin\theta_1 \end{cases} \quad (A.2)$$

Appendix B

- Kinematic equations

For torque-angular displacement (rotation) hysteresis loops, we must transform the tangential acceleration delivered by the accelerometers into angular acceleration. The relationship between tangential acceleration γ_A, γ_B and γ_C successively in A, B and C and the angular acceleration $\ddot{\theta}_1$, $\ddot{\theta}_2$ and $\ddot{x}_1$ are given by the following equations:

$$\vec{\gamma}_A = \ddot{x}_1\vec{X}_0 + d_1\ddot{\theta}_1\vec{X}_0 \quad (B.1)$$

$$\vec{\gamma}_B = \ddot{x}_1\vec{X}_0 + d_2\ddot{\theta}_1\vec{X}_0 \quad (B.2)$$

The acceleration at point O belongs to the first beam P_1 (lower beam) given by:

$$\overrightarrow{\gamma_{O\in P1}} = \ddot{x}_1\overrightarrow{X_0} + d_3\ddot{\theta}_1\overrightarrow{X_0} \quad (B.3)$$

The acceleration at point O, part of the second beam P_2 (upper beam), is given by:

$$\overrightarrow{\gamma_{O\in P2}} = \ddot{x}_2\overrightarrow{X_0} - d_5\ddot{\theta}_2\overrightarrow{X_0} \quad (B.4)$$

with $\ddot{x}_2$ acceleration at the center of gravity of the second beam (point G2)

$$\overrightarrow{\gamma_C} = \ddot{x}_2\overrightarrow{X_0} + d_4\ddot{\theta}_2\overrightarrow{X_0} \quad (B.5)$$

From Eqs. (B.1) and (B.2) we obtain:

$$\Rightarrow \begin{cases} \ddot{\theta}_1 = \frac{\overrightarrow{\gamma_A} - \overrightarrow{\gamma_B}}{d_1 - d_2} \\ \ddot{x}_1 = \frac{1}{2}(\overrightarrow{\gamma_A} + \overrightarrow{\gamma_B} - (d_1+d_2)\ddot{\theta}_1) \end{cases} \quad (B.6)$$

On the other hand, we obtain

$$\overrightarrow{\gamma_{O\in P1}} = \overrightarrow{\gamma_{O\in P2}} \quad (B.7)$$

$$\Rightarrow \ddot{x}_1 + d_3\ddot{\theta}_1 = \ddot{x}_2 - d_5\ddot{\theta}_2 \quad (B.8)$$

This gives us

$$\Rightarrow \ddot{x}_2 = \ddot{x}_1 + d_3\ddot{\theta}_1 + d_5\ddot{\theta}_2 \quad (B.9)$$

From Eqs (B.3), (B.4), (B.5), and (B.9) we obtain:

$$\Rightarrow \begin{cases} \ddot{\theta}_2 = \frac{\overrightarrow{\gamma_C} - \overrightarrow{\gamma_{O\in P1}}}{(d_4+d_5)} \\ \ddot{x}_2 = \frac{1}{2}(\overrightarrow{\gamma_{O\in P2}} + \overrightarrow{\gamma_C} - (d_4-d_5)\ddot{\theta}_2) \end{cases} \quad (B.10)$$

References

Ahmadian, H., Jalali, H., 2007. Identification of bolted lap joints parameters in assembled structures. Mech. Syst. Signal Process. 21, 1041–1050.

Beards, C., Williams, J., 1977. The damping of structural vibration by rotational slip in joints. J. Sound Vib. 53, 333–340.

Berthillier, M., Dupont, C., Mondal, R., Barrau, J., 1998. Blades forced response analysis with friction dampers. Trans. Am. Soc. Mech. Eng. 120, 468–474.

Bhagat, S., Bijoy, K.N., 2012. Identification of damping mechanism in layered and welded structure. Int. J. Mech. Sci. 63, 37–47.

Blau, P.J., 1992. Friction, lubrication and wear technology. ASM Handbook, vol. 18. ASM International, pp. 333–470.

Bouchaala, N., Dion, J.L., Peyret, N., Haddar, M., 2013. Micro-slip induced damping in the contact of nominally flat surfaces. Int. J. Appl. Mech. 5, 1350005 (20 pages).

Caignot, A., Ladeveze, D., Neron, S., Romeuf, T., 2005. Prediction of damping in space launch vehicles using a virtual testing strategy. In: 6th International Symposium on Launcher Technologies.

Davies, M., Barber, J.B., Hills, D., 2012. Energy dissipation in a frictional incomplete contact with varying normal load. Int. J. Mech. Sci. 55, 13–21.

Dini, D., Hills, D.A., 2009. Frictional energy dissipation in a rough Hertzian contact. J. Tribol. 131, 021401.

Dion, J.L., Chevallier, G., Peyret, N., 2012. Improvement of measurement techniques for damping induced by micro-sliding. Mech. Syst. Signal Process. 34, 106–115.

Eriten, M., Polycarpou, A.A., Bergman, L.A., 2010. Physics-based modeling for partial slip behavior of spherical contacts. Int. J. Solids Struct. 47 (18–19), 2554–2567.

Eriten, M., Polycarpou, A.A., Bergman, L.A., 2011. Physics-based modeling for fretting behavior of nominally flat rough surfaces. Int. J. Solids Struct. 48 (10), 1436–1450.

Gaul, L., 2000. Friction control for vibration suppression. Mech. Syst. Signal Process. 14 (2), 139–150.

Goodman, L., Klumpp, J., 1956. Analysis of slip damping with reference to turbine_blade vibration. Appl. Mech. Div.

Greenwood, J.A., Williamson, J.B.P., 1966. Contact of nominally flat surfaces. Proc. R. Soc. London A 295, 300–319.

Ibrahim, R.A., Pettit, C.L., 2005. Uncertainties and dynamic problems of bolted joints and others fasteners. J. Sound Vib. 279, 857–936.

Mindlin, R.D., 1949. Compliance of elastic bodies in contact. J. Appl. Mech. 16, 259–268.

Nanda, B.K., 2006. Study of the effect of bolt diameter and washer an damping in layered and jointed structures. J. Sound Vib. 290, 1290–1314.

Ouyang, H., Oldfield, M.J., Mottershead, J.E., 2006. Experimental and theoretical studies of a bolted joint excited by a tortional dynamic load. Int. J. Mech. Sci. 48, 1447–1455.

Peyret, N., Dion, J.L., Chevallier, G., Argoul, P., 2010. Micro-slip induced damping in planar contact under constant and uniform normal stress. Int. J. Appl. Mech. 2, 281–304.

Poudou, O., 2007. Modeling and Analysis of the Dynamics of Try-friction-clamped Structural Systems (Ph.D. thesis). University of Michigan.

Rao, J.S., Narayan, R., Rejin, R., 2010. Analytical estimation of microslip damping in bladed-disks. In: 5th International Conference, Brussels, Belgium, pp. 27–28.

Robbe-Valloire, F., Progri, R., Paffoni, B., Gras, R., 2000. Modélisation de la topologie micro-géométrique. Matériaux et Techniques, 3–4.